Formation and Maintenance of the Tropical Cold-Point Tropopause in a Dry Dynamic-Core GCM

JOOWAN KIM*

Department of Atmospheric and Oceanic Sciences, McGill University, Montreal, Quebec, Canada

SEOK-WOO SON

School of Earth and Environmental Sciences, Seoul National University, Seoul, South Korea

(Manuscript received 16 November 2014, in final form 6 April 2015)

ABSTRACT

The formation of the tropical cold-point tropopause (CPT) is examined using a dry primitive equation model driven by the Held–Suarez forcing. Without moist and realistic radiative processes, the dry model successfully reproduces the zonal-mean structure of the CPT. The modeled CPT is appreciably colder (~10 K) than the prescribed equilibrium temperature, and it is maintained by upwelling in the tropical upper troposphere and lower stratosphere (UTLS). A transient simulation starting from an axisymmetric steady state without the CPT shows that the evolution and maintenance of the CPT are closely related to the zonal-mean-flow response to wave driving in the stratosphere. The transformed Eulerian-mean analysis indicates that the wave driving is mostly due to convergence of synoptic-scale waves originating from the midlatitude troposphere and propagating into the subtropical UTLS in this model simulation. The modeled CPT also shows a large sensitivity to increased baroclinicity in the equilibrium temperature. Although planetary-scale waves are not considered in this simulation, the result confirms that wave-driven upwelling in the tropical UTLS is a crucial process for the formation and maintenance of the CPT. In addition, it also implies that synoptic-scale waves may play a nonnegligible role in this mechanism, particularly in the seasons when planetary-scale wave activity in the lower stratosphere is weak.

1. Introduction

In the tropics, the temperature lapse rate suddenly changes its sign at ~17 km, forming a sharp local minimum in the temperature profile. This sharp temperature minimum, the so-called cold-point tropopause (CPT), is a distinctive characteristic of the tropical tropopause and has interesting implications in various climate processes. As an important example, the thermal property of the CPT is intimately connected to the stratosphere–troposphere exchange process, which could significantly affect Earth's radiation budget by modifying the atmospheric composition. In particular, temperature of the CPT plays a crucial role in setting the amount of the water vapor in the stratosphere (Mote et al. 1996; Randel and Jensen 2013) and cirrus clouds in the tropical tropopause layer (Davis et al. 2013). These are very important atmospheric properties that affect the surface climate through radiation process (Forster and Shine 2002; Solomon et al. 2010).

Since the discovery of the tropopause in the midlatitude and tropics in early twentieth century [see the historical review by Labitzke and van Loon (1999)], its formation and maintenance were interesting physical and dynamical problems that have long been studied (Manabe and Strickler 1964; Highwood and Hoskins 1998; Seidel et al. 2001; Thuburn and Craig 2002; Fueglistaler et al. 2009; and references therein). Early studies have primarily considered radiative and convective processes. Manabe and Strickler (1964), for example, have successfully reproduced the vertical temperature profile in the tropics by combining radiative–convective equilibrium state in the troposphere and radiative

* Current affiliation: National Center for Atmospheric Research, Boulder, Colorado.

Corresponding author address: Joowan Kim, National Center for Atmospheric Research, P.O. Box 3000, Boulder, CO 80307.
E-mail: joowan@ucar.edu

DOI: 10.1175/JAS-D-14-0338.1

equilibrium state in the stratosphere. Extending this study, Thuburn and Craig (2002) suggested that the thermal structure near the tropical tropopause can be largely explained by the radiative effects of CO_2 and O_3. In addition, the importance of H_2O in the radiation budget of the upper troposphere and lower stratosphere (UTLS) is also stressed recently (T. Birner 2014, personal communication). These studies, however, offer only a limited explanation on the thermal structure because the resulting CPT is considerably warmer than the observed one (e.g., Gettelman et al. 2004; Fueglistaler et al. 2009). More importantly, observations show a localized layer of radiative heating instead of cooling near the CPT [$\sim$0.3 K day^{-1}; cf. Fig. 12b in Fueglistaler et al. (2009)], and this implies that radiative process alone cannot explain the sharp cold peak in the observation.

Beyond the radiative equilibrium, the sharp CPT has been explained by two key processes: diabatic cooling associated with deep convection and cirrus clouds near the tropopause and adiabatic cooling associated with tropical upwelling in the UTLS. The idea of deep convection and cirrus clouds explains the CPT by convective overshooting and cloud-top detrainment followed by physical cooling (Sherwood and Dessler 2003; Küpper et al. 2004; Kuang and Bretherton 2004) or hydrostatic adjustment at the tropopause level to the convective heating below (Holloway and Neelin 2007). These ideas are supported by strong coherence between the locations of deep convection and temperature minima at the CPT (e.g., Johnson and Kriete 1982; Gettelman et al. 2002; Kim and Son 2012) and works successfully in explaining the local or regional cooling of the CPT.

The other mechanism is based on adiabatic cooling by wave-driven upwelling across the CPT. This idea focuses on explaining the global (zonal mean) structure of the CPT. The upwelling is essentially a part of the stratospheric Brewer–Dobson circulation (BDC; Brewer 1949; Dobson 1956), which is driven by wave forcing both in the extratropical stratosphere (deep branch of the BDC; Garcia 1987; Yulaeva et al. 1994; Holton et al. 1995; Plumb and Eluszkiewicz 1999) and in the subtropical lower stratosphere (shallow branch of the BDC; Randel et al. 2008; Birner and Bönisch 2011; Garny et al. 2011). The deep branch of the BDC is driven by planetary-scale and gravity waves that propagate and break in the middle and upper stratosphere (e.g., Holton et al. 1995; Plumb 2002), and the shallow branch is organized by planetary- and synoptic-scale waves that are trapped and break in the tropical UTLS (Plumb 2002; Birner and Bönisch 2011; Abalos et al. 2014 for transient response). Recent studies have shown that CPT temperature is more closely related to the shallow branch than the deep branch of the BDC (Garny et al. 2011; Ueyama et al. 2013; Grise and Thompson 2013).

The formation and maintenance mechanisms of the CPT may be an essential part to understanding its role of the CPT in general circulation and global climate change. Although many processes affect the CPT as described above, the zonal-mean structure of the CPT is largely determined by the balance between radiative (or radiative–convective) heating and dynamic cooling. In fact, the zonal-mean structure is qualitatively well reproduced in a dry general circulation model (GCM) experiment, even without detailed convective and radiative processes. One good example is the Held and Suarez experiment (Held and Suarez 1994, hereinafter HS) shown in Fig. 1. The dry primitive equation model driven by thermal relaxation toward an axisymmetric equilibrium temperature (Fig. 1a) generates the well-defined CPT around 100 hPa (Fig. 1b), although no CPT is prescribed in the equilibrium temperature (Fig. 1a). A similar result has been presented in several idealized modeling studies (Chen and Sun 2011; Haqq-Misra et al. 2011; Ueyama et al. 2013). However, no systematic study has been made to understand the formation of the CPT in the HS-type experiments in spite of its extensive use in the atmospheric general circulation studies (e.g., Polvani and Kushner 2002; Son and Lee 2005; Butler et al. 2010; Chen and Sun 2011).

In this context, the present study revisits the HS experiment and documents the dynamical mechanism of the CPT formation and maintenance in the HS-like simulations. The formation mechanism is examined using the transformed Eulerian-mean (TEM) framework focusing on wave-driven circulation, and the effectiveness of wave forcing in this mechanism is tested. Both axisymmetric (eddy free) and nonaxisymmetric (eddy permitting) simulations are made in order to understand the net effect of wave forcing. The temporal evolution of the CPT is further examined by conducting a transient simulation starting from an initial state that does not have the CPT. In short, it is found that adiabatic cooling by wave-driven upwelling in the tropical UTLS is the key mechanism of the CPT formation, and this upwelling is mainly driven by the convergence of synoptic-scale waves in the subtropical UTLS.

In next section, the model and experiment design are briefly described. Key results are then presented in section 3. In section 4, the robustness of the results is tested using a suite of sensitivity experiments. Finally, section 5 summarizes overall findings of this study and discusses their implication to the observed CPT.

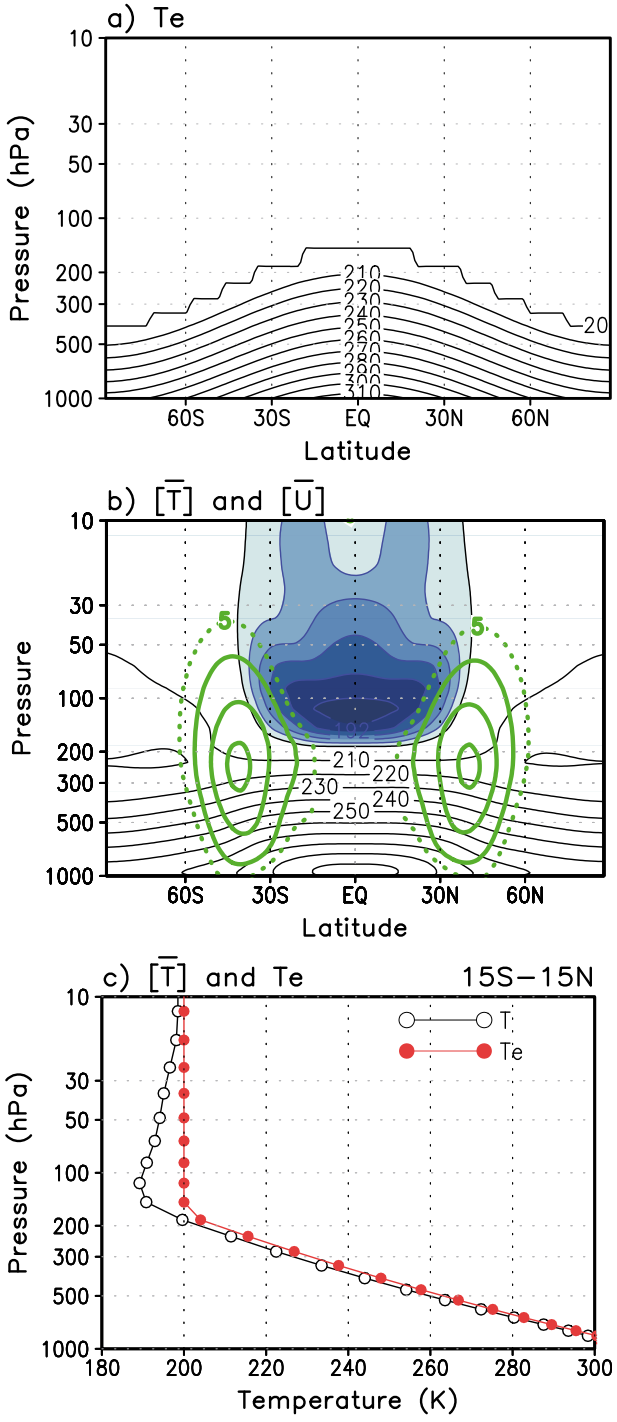

FIG. 1. (a) Radiative equilibrium temperature (T_e; K) and (b) zonal-mean zonal wind (m s^{-1}; thick contour) and temperature (K; thin contour and shading) of the climatology. Shading interval is 2 K. (c) Vertical profiles of the T_e (closed circle) and temperature (open circle) in the deep tropics (15°S–15°N).

2. Dynamic-core GCM experiments

a. Control simulation

We use a dry dynamic-core GCM developed by the Geophysical Fluid Dynamics Laboratory (GFDL). It solves the primitive equations on terrain-following σ coordinates using a spherical-transform method. The control simulation is made at T42 resolution with 40 unequally spaced σ levels, which is defined in Chen and Zurita-Gotor (2008). The model top is 0.01 hPa, and 20 levels are located above 100 hPa. To prevent artificial wave reflection from the model top, a sponge layer is used for the model levels above 0.5 hPa as in Chen and Zurita-Gotor (2008).

The control run is made with the HS forcing as defined in HS. Briefly, the model is forced by relaxing toward a prescribed axisymmetric temperature T_e and dissipated by internal diffusion and Rayleigh friction near the surface. The HS T_e is given as

$$T_e(\phi,p) = \max\left\{200K, \left[T_0 - \Delta_h \sin^2\phi - \Delta_v \log\left(\frac{p}{p_0}\right)\cos^2\phi\right]\left(\frac{p}{p_0}\right)^{\kappa}\right\}, \quad (1)$$

where T_0 is the surface temperature at the equator (315 K), Δ_h is an equator-to-pole temperature difference at the surface (60 K), Δ_v is a static stability parameter (10 K), φ is the latitude, $\kappa = 2/7$, and $p_0 = 1000$ hPa. The T_e has statically stable but baroclinically unstable thermal structure; thus, eddies primarily develop through baroclinic instability. The relaxation time scale τ is 4 days at the equatorial surface and gradually increases up to 40 days in the high latitudes or above the middle troposphere (for more detail, refer to HS). For internal diffusion, the eighth-order hyperdiffusion is used with a damping time scale of 0.1 days for the smallest spherical harmonics. Gravity wave drag is not included in the model. All simulations are made for 10 000 days with perpetual equinox conditions, of which the last 9000 days are used for the climatology and analyses. No seasonality is considered in the simulations.

b. Axisymmetric simulation

To isolate the thermally driven circulation, the model is also integrated with an axisymmetric (2D) configuration. In the same model, zonal waves are truncated at wavenumber 0; thus, no wave exists in the zonal direction, while both the meridional and vertical resolutions are kept the same as in the control run (T42, 40 levels). This simple treatment, however, results in significant oscillations in the subtropical circulation (Held and Hou 1980; Kim and Lee 2001; Son and Lee 2005;

Bordoni and Schneider 2010). This is mainly due to the local inertial instability developing in the course of the model integration. To reduce this instability, the second-order vertical diffusion is added to the momentum and thermodynamic equations as in Held and Hou (1980), and surface drag is used instead of Rayleigh friction for the bottom boundary as in Kim and Lee (2001). Specifically, a constant kinematic diffusivity ν of $0.4\,\mathrm{m^2\,s^{-1}}$ is used for vertical diffusion of the zonal and meridional momentum. The same coefficient is also applied to the potential temperature by assuming the Prandtl number of 1.

The axisymmetric run reaches steady state very quickly even with the weak vertical diffusion, but the weak vertical diffusion does not fully suppress the local instability in all experiments; noticeable wiggles still exist in temperature and wind field although they are in steady state. To damp this noise in the axisymmetric run, previous studies have used a high vertical diffusion coefficient up to 3–$5\,\mathrm{m^2\,s^{-1}}$ (e.g., Bordoni and Schneider 2010). This strong diffusion does not change the qualitative result of the axisymmetric simulation. However, it significantly affects the companion nonaxisymmetric (3D) simulation, which uses the same vertical diffusion for comparison purpose. With the strong vertical diffusion, the modeled CPT broadens out in the vertical direction, and the associated westerly jet extends into the upper stratosphere because meridional temperature gradient is weakened in the subtropical UTLS. This is unrealistic; thus, the small vertical diffusion, $\nu = 0.4\,\mathrm{m^2\,s^{-1}}$ is used for the axisymmetric and accompanying nonaxisymmetric simulations. Note that vertical diffusion is used only for axisymmetric simulation and its companion nonaxisymmetric simulation. No vertical diffusion is applied to the control simulation and sensitivity runs described below.

c. Transient simulation

The time evolution of the CPT is also investigated by integrating the model from an initial condition that does not have the CPT. The same configuration as in control simulation is used for the transient simulation except for the initial condition. The initial condition is basically obtained from the axisymmetric steady state, but instead of simply using the axisymmetric steady state, the initial condition is slightly modified using the procedure described in Branscome et al. (1989). Briefly, it finds a balanced state that can be steady solution of the model using a given temperature field and by setting meridional wind to zero. Temperature field from the axisymmetric steady state is used for this computation. Based on this balanced state, a total of 40 ensemble members are generated by adding random perturbations to the vorticity field at the lowest three model levels. The maximum size of the perturbation is $10^{-7}\,\mathrm{s^{-1}}$, which is roughly 0.1% of the planetary vorticity in the midlatitude. The simple ensemble mean is used for the analysis. This experiment effectively reveals the formation process of the CPT and the role of baroclinic eddies in the process.

d. Sensitivity tests

The robustness of the finding is further tested by integrating the model with different resolutions. Both horizontal and vertical resolutions are systematically changed. The sensitivity to the choice of the T_e profile itself is also tested. As in Son et al. (2007), another T_e profile proposed by Schneider and Walker (2006, hereinafter SW) is tested. The SW T_e is similar to the HS T_e. However, it is statically unstable (e.g., Fig. 1 in Son and Polvani 2007) and uses a dry convective adjustment to stabilize the temperature profile when the atmosphere becomes statically unstable. The convective adjustment has a much shorter time scale (4 h) than the radiative equilibrium (10–40 days), and it mimics the radiative–convective equilibrium in a more realistic way, although it is still very simplified process. We used the parameters of the Earth-like simulation in SW, unless indicated otherwise. These sensitivity tests are documented in section 4.

3. Results

a. Thermodynamic balance

Figure 1 shows the HS T_e and simulated zonal-mean climatology (temperature and zonal wind) from the control run. The climatology presents the tropospheric jets centered near 40° at 250 hPa in both hemispheres with poleward redistribution of heat in the troposphere. As already discussed, it shows the distinct CPT around ~100 hPa in the tropics (114 hPa at model level) with a minimum zonal-mean temperature below 190 K (Figs. 1b,c). This temperature is roughly 10 K colder than the T_e, to which the temperature keeps relaxed (Fig. 1c). Given the fact that the thermal relaxation toward the T_e is balanced by dynamic heating/cooling in the climatological steady state, it is naturally inferred that the CPT shown in Fig. 1b is formed by dynamic cooling in the tropical UTLS.

The thermal balance can be readily examined using the TEM thermodynamic equation in log-pressure coordinate,

$$\frac{\partial\overline{\theta}}{\partial t}+\frac{1}{a}\frac{\partial\overline{\theta}}{\partial\phi}\overline{v}^{*}+\frac{\partial\overline{\theta}}{\partial z}\overline{w}^{*} = -\frac{1}{\rho_0}\frac{\partial}{\partial z}[\rho_0(\overline{\theta}_{\phi}\overline{v'\theta'}/a\overline{\theta}_{z}+\overline{w'\theta'})]+\overline{Q}, \qquad (2)$$

where the overbar represents the zonal mean, and the prime is a perturbation from the zonal mean. All other symbols are standard, as in Andrews et al. (1987). The

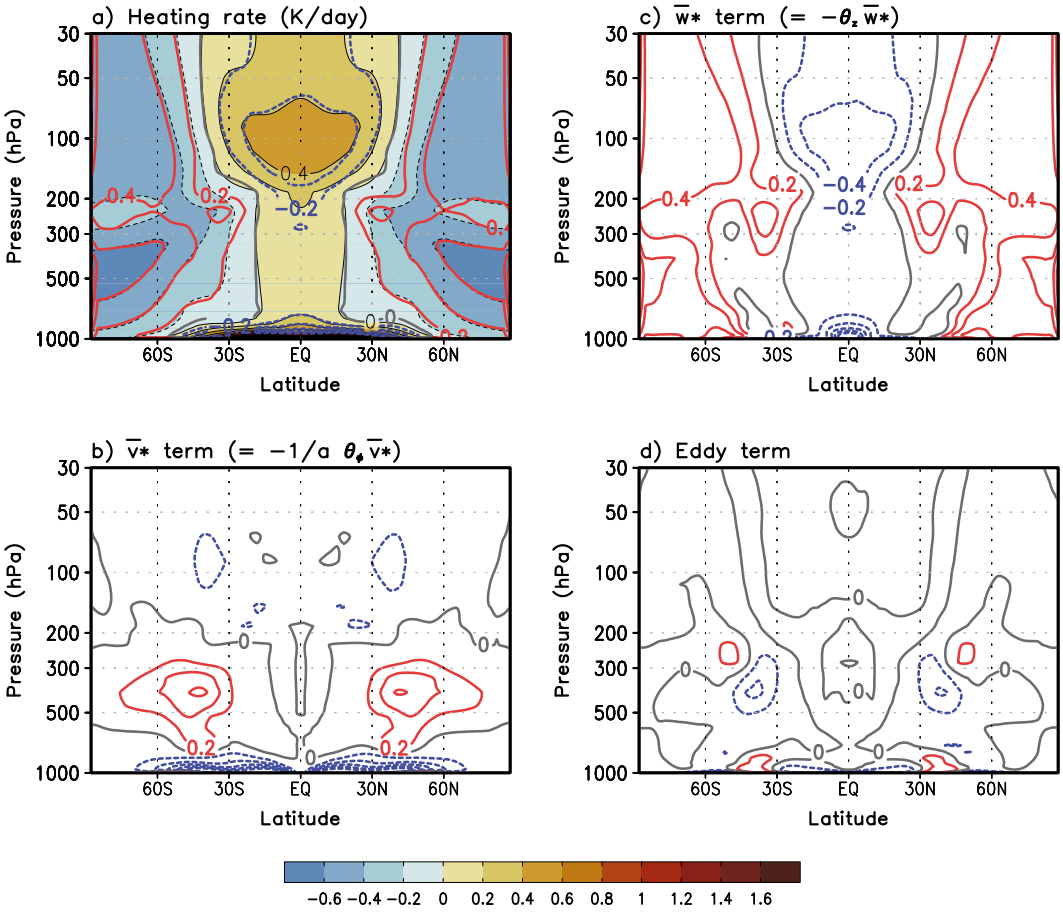

FIG. 2. (a) Zonal-mean heating rates (K day^{-1}) by external thermal forcing (shading) and dynamics (contour). The dynamic heating decomposed into (b) horizontal and (c) vertical advection by the residual circulation and (d) vertical eddy heat flux term.

zonal-mean diabatic heating is $\overline{Q}$, defined as $\overline{Q} = -(\overline{\theta} - \overline{\theta}_e)/\tau$ in the HS experiment, where $\theta_e = T_e e^{\kappa z/H}$ with $\kappa = 2/7$ and $H = 7$ km. The TEM residual velocities on the left-hand side are defined as

$$\overline{v}^* \equiv \overline{v} - \frac{1}{\rho_0}\frac{\partial}{\partial z}(\rho_0 \overline{v'\theta'}/\overline{\theta}_z) \quad \text{and} \tag{3}$$

$$\overline{w}^* \equiv \overline{w} + \frac{1}{a\cos\phi}\frac{\partial}{\partial \phi}(\cos\phi \overline{v'\theta'}/\overline{\theta}_z), \tag{4}$$

where a is the radius of Earth (6371 km) and $\rho_0 = \rho_s e^{-z/H}$ with ρ_s the reference surface density (1.48 kg m^{-3}; this value does not affect the result). For a long-term mean, the local tendency term $\partial\overline{\theta}/\partial t$ can be neglected, and Eq. (2) may be written as

$$\frac{1}{a}\frac{\partial \overline{\theta}}{\partial \phi}\overline{v}^* + \frac{\partial \overline{\theta}}{\partial z}\overline{w}^* + \frac{1}{\rho_0}\frac{\partial}{\partial z}[\rho_0(\overline{\theta}_\phi \overline{v'\theta'}/a\overline{\theta}_z + \overline{w'\theta'})] \simeq -\frac{\overline{\theta} - \overline{\theta}_e}{\tau}. \tag{5}$$

It suggests that the external thermal forcing term on the right-hand side should balance the dynamic forcing terms on the left-hand side.

Figure 2a shows that the external heating [shading; the right-hand-side term of Eq. (5)] is well balanced by dynamic forcing [contour; sum of the left-hand-side terms of Eq. (5)] in the steady state. The external forcing tends to warm the tropics but cool the extratropics, roughly mimicking the basic role of the radiative forcing in the atmosphere. Except for the near-surface heating, the maximum external warming is found in the tropical UTLS (Fig. 2a). Since the model is relaxed to roughly isothermal temperature (200 K; see Fig. 1c) in the tropical UTLS, this warming is a response to the colder temperature (<200 K) in the tropical UTLS produced by dynamic cooling. This balance is similar to the result from a free-running GCM (WACCM) in Abalos et al. (2013).

The above result suggests that the formation of the CPT in the model can be understood by examining the

thermal balance. Figure 2a also shows that the thermal balance in the upper troposphere and stratosphere is to some extent separated from that in the middle and lower troposphere. For example, dynamic cooling (and external heating) in the tropical UTLS is well separated from the near-surface cooling that is confined within the boundary layer. Similarly, dynamic warming in the extratropical stratosphere is also separated from that in the troposphere by the local minimum around the tropopause. These results suggest that the zonal-mean temperature in the upper troposphere and stratosphere, especially above 250 hPa, may be determined by different process(es) compared to that controls the troposphere in the model.

The decomposition of dynamic forcing further clarifies this question. Figures 2b–d show the three dynamic terms on the left-hand side of Eq. (5), respectively. They clearly show that the strong dynamic cooling in the tropical UTLS is mostly caused by adiabatic cooling due to tropical upwelling (Fig. 2c). This contrasts to the near-surface cooling over 60°S–60°N, which is mainly caused by the cold advection from the surface residual circulation (Fig. 2b). It is noteworthy that most of dynamic heating in the stratosphere is driven by adiabatic heating (Fig. 2c), while a large portion of the tropospheric heating is caused by meridional temperature advection, particularly in the midlatitude (Figs. 2b). Note a qualitatively similar dynamic forcing is also found in a comprehensive GCM (CMAM; Birner 2010). As shown in Fig. 2d, the contribution of leftover eddy terms to the thermodynamic budget—that is, the third term on the left-hand side of Eq. (5)—is rather minor in our simulation. Essentially no contribution is found in the stratosphere.

Tropical upwelling in the UTLS is illustrated in Fig. 3a in terms of the streamfunction. In this region, streamlines cross the isentropes, and associated upwelling causes adiabatic cooling over the broad region from 30°S to 30°N. Although this upwelling decays rapidly with height, the strong stratification above 150 hPa results in the maximum adiabatic cooling at around 100 hPa (Fig. 3c). Since the stratification is partly forced by the T_e profile (Fig. 1c), this result suggests that tropical upwelling across the prescribed tropopause is the key factor that determines the maximum dynamic cooling in the tropical UTLS and the formation of the CPT in this simulation.

Figure 3a also shows that tropical upwelling is a part of the BDC in the model. Upwelling is evident in the tropical lower stratosphere (above 100 hPa), and downwelling is predominant in the high-latitude stratosphere. This feature resembles the BDC in the atmosphere although this model misses the deep branch owing to lack of the background westerly in the stratosphere. It is also clearly shown from Fig. 3b that the waves propagate upward up to ~50 hPa around the westerly jet (EP-flux vectors). These vertically propagating waves play a crucial role in driving the BDC. As discussed later, these waves are dominated by the synoptic scale as there is no source of planetary-scale wave in the model. It might be considered that synoptic-scale waves are less efficient than planetary-scale waves in driving large-scale circulation in the stratosphere as their critical level is located at lower altitude compared to that of planetary-scale waves (Charney and Drazin 1961). However, recent studies have shown that they can still drive a notable BDC in an idealized GCM (e.g., Chen and Sun 2011; Haqq-Misra et al. 2011; Ueyama et al. 2013).

b. *Tropopause upwelling*

The nature of tropical upwelling is further examined in this section. Tropical upwelling, in terms of the residual vertical velocity $\overline{w}^*$, can be reproduced by using TEM mass continuity and momentum equations (e.g., Haynes et al. 1991; Randel et al. 2002; Kerr-Munslow and Norton 2006):[1]

$$\frac{1}{a\cos\phi}\frac{\partial(\overline{v}^*\cos\phi)}{\partial\phi}+\frac{1}{\rho_0}\frac{\partial\rho_0\overline{w}^*}{\partial z}=0 \quad \text{and} \tag{6}$$

$$\frac{\partial\overline{u}}{\partial t}-\overline{\eta}\overline{v}^*+\frac{\partial\overline{u}}{\partial z}\overline{w}^*=\mathrm{DF}+\overline{X}, \tag{7}$$

where $\overline{\eta}=f-(a\cos\phi)^{-1}(\overline{u}\cos\phi)_\phi$ is the absolute vorticity of the zonal-mean flow, $\mathrm{DF}=[1/(\rho_0 a\cos\phi)]\mathbf{\nabla}\cdot\mathbf{F}$ is the scaled Eliassen–Palm flux (EP flux) divergence, and $\overline{X}$ represents forces by unresolved processes. By averaging the mass continuity equation [Eq. (6)] over a latitude band $(-\phi_0,\phi_0)$, and integrating it in vertical from the top to a certain level z, we can obtain tropical mean vertical velocity over the latitude band as follows:

$$\langle\overline{w}^*\rangle(z)=\frac{\cos\phi_0}{\rho_0(z)a\displaystyle\int_{-\phi_0}^{+\phi_0}\cos\phi\,d\phi}\int_z^\infty\rho_0(z')[\overline{v}^*(\phi_0,z')-\overline{v}^*(-\phi_0,z')]\,dz'. \tag{8}$$

Here angle brackets denote latitudinal average over $-\phi_0$ to ϕ_0. The vertical velocity $\overline{w}^*$ is assumed to be

[1] The method used in Kerr-Munslow and Norton (2006) is slightly different from that in Haynes et al. (1991) in that $\overline{u}_z\overline{w}^*$ term is explicitly used to estimate the meridional wind $\overline{v}^*$. Haynes et al. (1991) implicitly considered this term by making vertical integration along a constant angular momentum line, although they finally neglect this term using quasigeostrophic assumption and made vertical integration along a constant latitude for computational simplicity. We tested the both methods, and found that the difference is negligibly small. The result presented in this study follows Haynes et al. (1991).

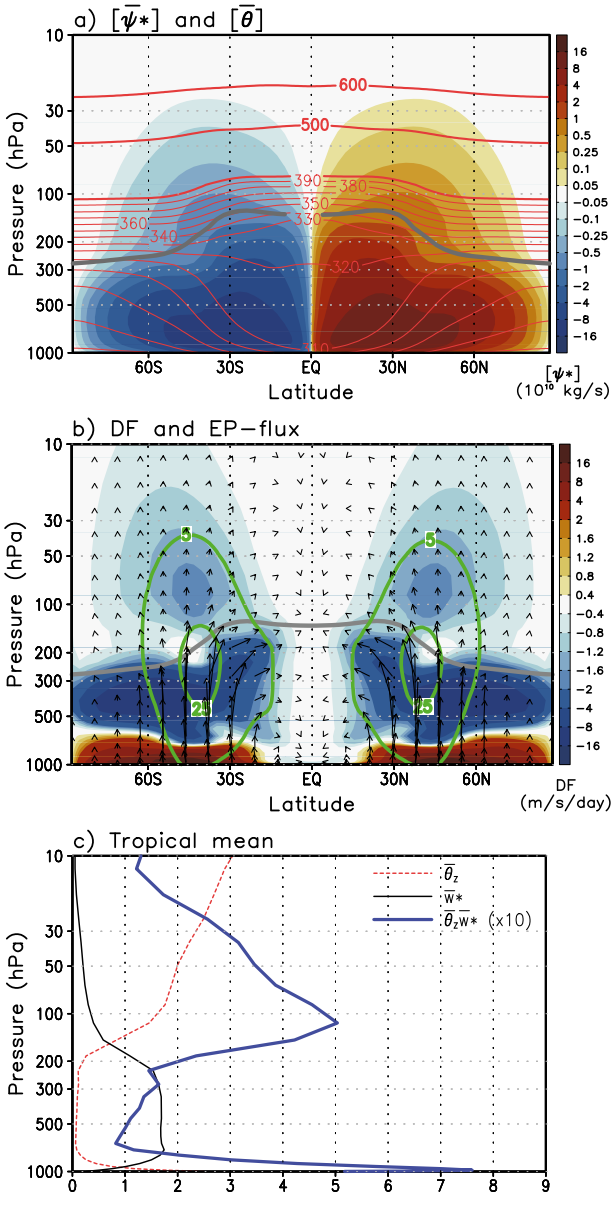

FIG. 3. (a) Mass streamfunction of the residual circulation (10^{10} kg s^{-1}; shading), potential temperature (K; contours). (b) EP flux (vector), scaled EP-flux divergence $[(\rho_0 a\cos\phi)^{-1}\nabla\cdot\mathbf{F}$; m s^{-1} day^{-1}; shading], and zonal-mean zonal wind (m s^{-1}; contour) of the climatology. (c) Vertical profiles of $\overline{\theta}_z$ (10^{-2} K m^{-1}; red), $\overline{w}^*$ (10^{-3} m s^{-1}; black), and $\overline{\theta}_z\overline{w}^*$ (K day^{-1}, scaled by 10; blue) in the deep tropics (15°S–15°N). The lapse-rate tropopause is shown in (a) and (b) as thick gray lines. EP-flux vectors are scaled in height in (b) by multiplying by $e^{z/H}$ for visual clarity.

zero at the top. Equation (8) indicates that latitude-mean vertical velocity at a given level $\langle\overline{w}^*\rangle(z)$ can be estimated from the meridional mass divergence at the latitude boundary integrated above the specified level. By rearranging Eq. (7), $\overline{v}^*$ can be derived as

$$\overline{v}^* = \frac{1}{\overline{\eta}}\left(\frac{\partial\overline{u}}{\partial t} + \frac{\partial\overline{u}}{\partial z}\overline{w}^* - \mathrm{DF} - \overline{X}\right). \tag{9}$$

If vertical integration of Eq. (8) is performed along a constant angular momentum line [refer to Haynes et al. (1991)] and neglecting the unresolved forcing $\overline{X}$, Eq. (8) may be expressed as below as in Randel et al. (2002):

$$\langle\overline{w}^*_m\rangle(z) = \frac{\cos\phi_0}{\rho_0(z)a\displaystyle\int_{-\phi_0}^{+\phi_0}\cos\phi\, d\phi} \times \int_z^\infty \rho_0(z')\left[\frac{1}{\overline{\eta}}\left(\frac{\partial\overline{u}}{\partial t} - \mathrm{DF}\right)_{\overline{m}}\right]_{-\phi_0}^{+\phi_0} dz', \tag{10}$$

where $\int(\cdot)_{\overline{m}}\,dz$ denotes integration along a constant angular momentum. Subscript m in $\langle\overline{w}^*_m\rangle$ indicates that this is upwelling estimated from the momentum equation. In this study, $\langle\overline{w}^*_m\rangle$ is estimated over the latitude band 15°S–15°N and vertical integration is made following a constant latitude instead of constant angular momentum. It is worth noting that the momentum balance can be ill defined near the equator because $\overline{\eta}$ becomes zero. However, the balance [Eq. (9)] is well satisfied at both 15°S and 15°N where the meridional mass flux is estimated.

Figure 4 presents $\langle\overline{w}^*_m\rangle$ estimated from Eq. (10) (thick black) along with $\langle\overline{w}^*\rangle$ directly computed from Eq. (4) at the CPT (thick gray). They are remarkably similar to each other in both the daily variation and long-term mean, indicating that tropical upwelling can be quantitatively evaluated by considering the local wind tendency and wave driving. The decomposition of $\langle\overline{w}^*_m\rangle$ into the contributions by wind tendency and the meridional and vertical EP-flux convergences further shows that tropical upwelling is largely explained by the meridional EP-flux convergence (thin red) with a rather minor but nonnegligible contribution of the vertical EP-flux convergence (thin blue).[2] The wind tendency is important in the short-term variability (<30 days). However, its contribution on time-mean $\langle\overline{w}^*_m\rangle$ is negligibly small. In general, the wind tendency term tends to balance wave forcing and partly reduce the fluctuation of $\langle\overline{w}^*_m\rangle$.

[2] The relative contribution of the vertical EP-flux convergence increases significantly for the latitude band of 30°S–30°N as wave forcing at the boundary is directly affected by the upward EP flux from the midlatitude lower troposphere. However, this separation may not be important in the sense that the horizontal and vertical EP fluxes are just geometrical separation of wave activity flux.

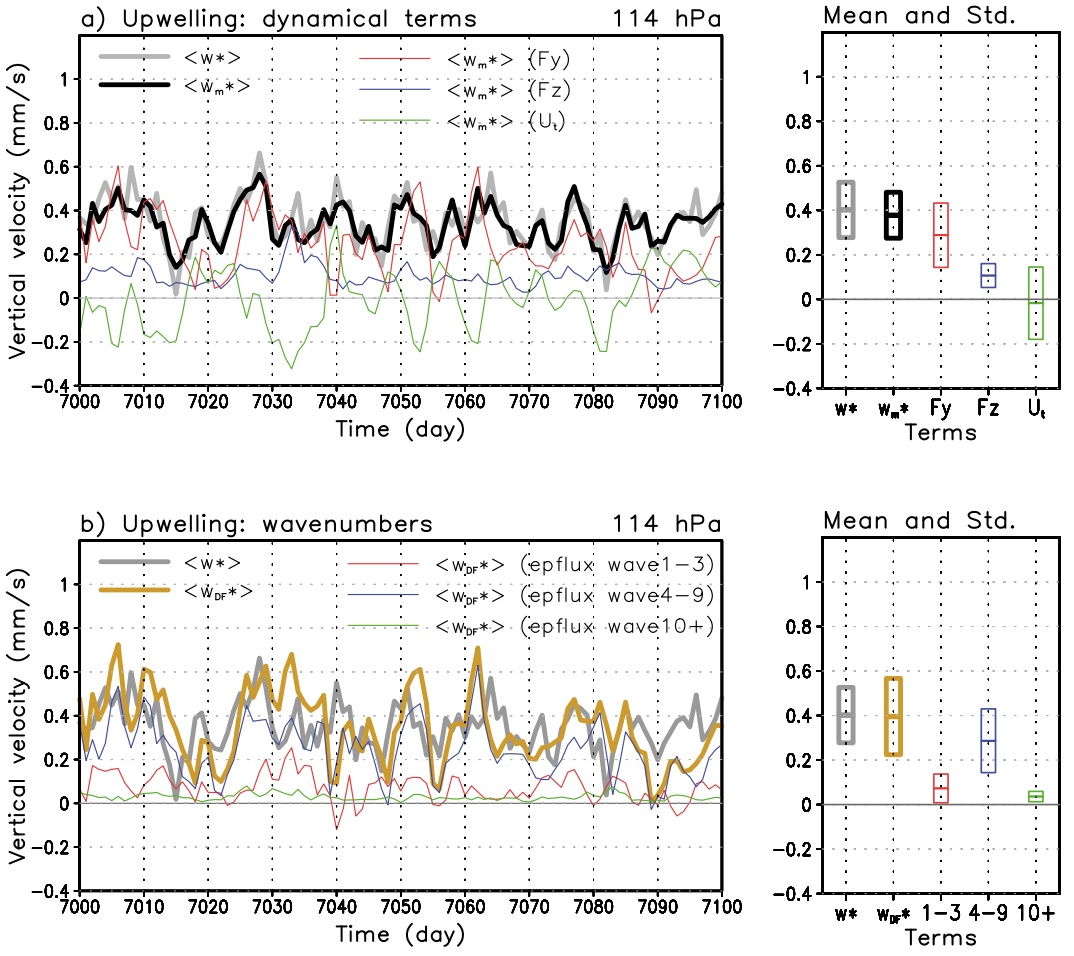

FIG. 4. Tropical-mean (15°S–15°N) residual vertical velocities at 114 hPa computed from the definition ($\langle \overline{w}^* \rangle$; thick gray), estimated from the momentum equation ($\langle \overline{w}^*_m \rangle$; thick black), and the same estimate with wave forcing only ($\langle \overline{w}^*_{\mathrm{DF}} \rangle$; thick yellow). (left) (a) $\langle \overline{w}^*_m \rangle$ by the horizontal (F_y; red) and vertical (F_z; blue) EP flux and zonal wind tendency ($\overline{u}_t$; green) and (b) $\langle \overline{w}^*_{\mathrm{DF}} \rangle$ by zonal wavenumbers 1–3 (red), 4–9 (blue), and 10 and larger (green) forcing. (right) Mean (center bar) and one standard deviation (box) for each estimate.

The potential role of the EP flux in driving $\langle \overline{w}^*_m \rangle$ is readily seen in Fig. 3. The Rossby waves, which propagate from the troposphere to the stratosphere, refract equatorward (vectors), resulting in the EP-flux convergence in the subtropical lower stratosphere. The associated easterly momentum deposit is then balanced by the Coriolis torque of the poleward motion ($\overline{v}^*$) in the subtropical stratosphere. This wave driving yields tropical upwelling as indicated in Eq. (8).

The above results indicate that tropical upwelling across the modeled CPT is primarily driven by wave forcing in the subtropical lower stratosphere. This wave-driven upwelling, estimated only from the EP-flux divergence $\langle \overline{w}^*_{\mathrm{DF}} \rangle$ (i.e., the wind tendency term neglected), is further decomposed into different zonal wavenumbers in Fig. 4b. The result shows that a large portion of tropical upwelling is due to synoptic-scale waves with zonal wavenumbers 4–9. This is not surprising because there is no external planetary wave source in the model.

How do synoptic-scale waves propagate into the lower stratosphere? This is likely a result of the vertically extended westerly jet in the model (Fig. 3b). Considering the quasigeostrophic refractive index n_k^2 on the beta plane, waves can propagate vertically in the regions where n_k^2 is positive (Charney and Drazin 1961; Dickinson 1968):

$$n_k^2 = \frac{\overline{q}_y}{\overline{u} - c} - k^2 - \frac{\varepsilon}{4H^2}, \tag{11}$$

where $\overline{q}_y$ is meridional gradient of background potential vorticity, k is a zonal wavenumber, and $\varepsilon = f_0^2/N^2$ with

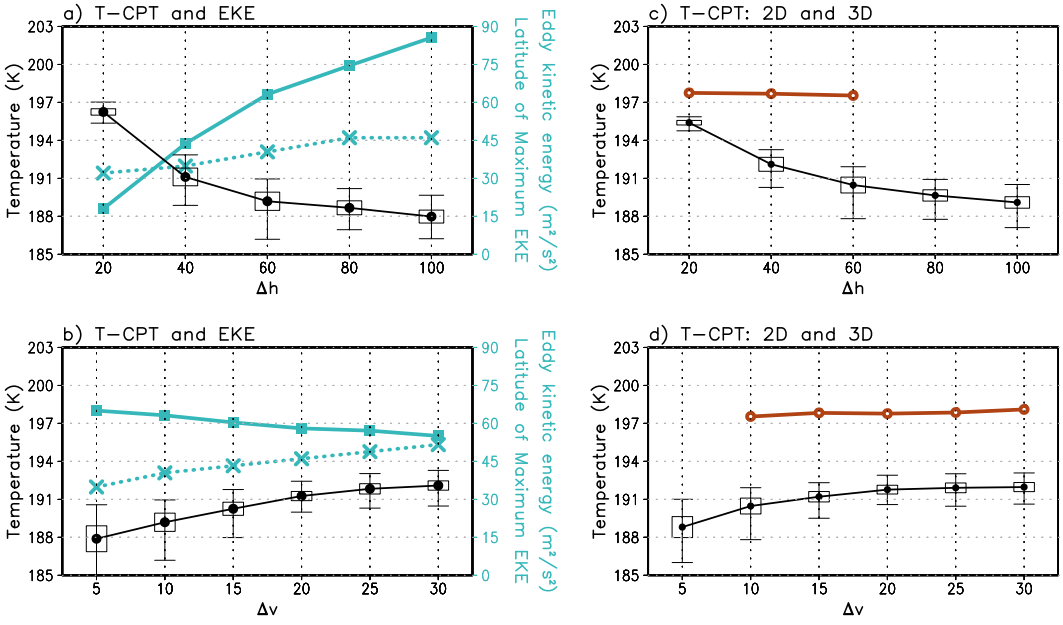

FIG. 5. Modeled CPT temperature in the deep tropics (15°S–15°N; circle) and global-mean eddy kinetic energy (EKE; square) and latitude of the EKE maximum (cross) as a function of (a) horizontal temperature gradient (Δ_h) and (b) static stability (Δ_v) parameters in the HS T_e. (c),(d) CPT temperatures from the axisymmetric (open circle) and corresponding eddy-permitting simulations (closed circle). Boxes denote one standard deviation and whiskers show minimum and maximum values.

the Coriolis parameter f_0 and buoyancy frequency N. This equation is identical to Eq. (4.5.28) of Andrews et al. (1987), and all symbols are standard. For synoptic-scale waves, whose phase speed is not negligible ($\sim 5\,\mathrm{m\,s^{-1}}$ in the subtropics; Randel and Held 1991), the first term on the right-hand side of Eq. (11) is large and synoptic waves with a relatively large wavenumber can still satisfy the propagating condition. As shown in Fig. 3b, the simulated westerly jet is extended in the vertical, and zonal wind at 100 hPa is faster than $5\,\mathrm{m\,s^{-1}}$ over 20°–60°N/S where wave activity is strong. This vertically extended westerly allows synoptic-scale waves to propagate farther upward (see EP-flux vectors in Fig. 3b).

c. *Sensitivity to baroclinicity*

It is so far shown that the CPT is formed by adiabatic cooling resulting from tropical upwelling in the UTLS. This upwelling is primarily driven by convergence of synoptic-scale waves in the tropical lower stratosphere. The robustness of this finding is tested in this section by performing a series of sensitivity runs with varying baroclinicity in the T_e profile. In the HS T_e, baroclinicity can be modulated by the two parameters that control meridional temperature gradient (Δ_h) and static stability (Δ_v) [Eq. (1)]. The baroclinicity is proportional to the vertical wind shear (or horizontal temperature gradient considering the thermal–wind relationship) and inversely proportional to the static stability. As such, the baroclinicity of the HS T_e can be increased by increasing Δ_h or decreasing Δ_v.

Figures 5a and 5b summarize the sensitivity of CPT temperature to the varying Δ_h and Δ_v. As expected from the results of the previous section, CPT temperature becomes colder as the baroclinicity increases (Δ_h increases or Δ_v decreases); it is anticorrelated with the baroclinicity of the T_e profile. More importantly, the modeled CPT temperatures show strong sensitivity to the background baroclinicity. In Fig. 5a, CPT temperature changes roughly 8 K in the range of Δ_h change. Particularly, it changes ~5 K when Δ_h is increased from 20 to 40 K. This strong sensitivity implies that baroclinic (largely synoptic scale) waves might be very influential in setting temperature at the CPT.

It may be worth to note that CPT temperature does not change much when Δ_h is large. This saturation of CPT temperature can partly be explained by the eddy activity, which is measured by total eddy kinetic energy (EKE). The location of the maximum EKE (dashed line with cross in Figs. 5a and 5b) shifts slightly poleward with increasing Δ_h. The location of the westerly jet also shows the same behavior. With this, the region of the maximum wave convergence in the subtropical lower stratosphere also shifts poleward, and this change makes

wave-driven upwelling slightly less efficient with increasing Δ_h, although still a larger wave convergence is observed at around 15° with increasing Δ_h due to an increased baroclinic eddy production in the midlatitude. In addition, the domain integrated EKE (solid line with square) does not change linearly with Δ_h as well. Its increment gets smaller with larger Δ_h, and this also partly contributes to the saturation of CPT temperature change.

Although the above result clearly shows that the modeled CPT is primarily driven by baroclinic eddies, it is still plausible that CPT temperature is in part modulated by the thermally driven overturning circulation without wave driving. This possibility is tested by integrating the model with an axisymmetric (eddy free) configuration. This configuration has been widely used in the study of the Hadley circulation (e.g., Held and Hou 1980). As described in section 2b, the weak vertical diffusion of $\nu = 0.4\,\mathrm{m^2\,s^{-1}}$ is applied to momentum and thermodynamic equations in order to obtain the stationary solution. This weak diffusion is also adopted for the companion nonaxisymmetric (3D and eddy permitting) runs. Note that all other nonaxisymmetric model simulations discussed above do not have vertical diffusion.

Figures 5c,d compare CPT temperatures from the axisymmetric simulations with those from the companion nonaxisymmetric simulations with vertical diffusion. Because the CPT is not well defined in the axisymmetric runs, the coldest temperature between 50 and 500 hPa is used for CPT temperature of the axisymmetric runs. All axisymmetric simulations that have the stationary solution show about 198-K CPT regardless of Δ_h and Δ_v. This result indicates that the contribution of the thermally driven circulation (i.e., vertical extension of the Hadley cell) to the CPT is negligible. The vertical diffusion in the nonaxisymmetric runs tends to increase CPT temperatures (cf. black dots in the left columns to those in the right). However, CPT temperature and its behavior with increasing baroclinicity is still well observed, and the CPT of the nonaxisymmetric runs is much colder than the one in the axisymmetric runs.

d. *Transient experiment*

In order to explore the CPT formation in more detail, the temporal evolution of temperature is further examined in the UTLS by integrating the nonaxisymmetric model from the balanced axisymmetric initial condition described in section 2c. The initial condition, which is obtained from axisymmetric simulation, has a strong subtropical jet that extends into the whole stratosphere by maintaining the thermal–wind balance (Fig. 6). A total of 40 ensemble simulations are made by integrating

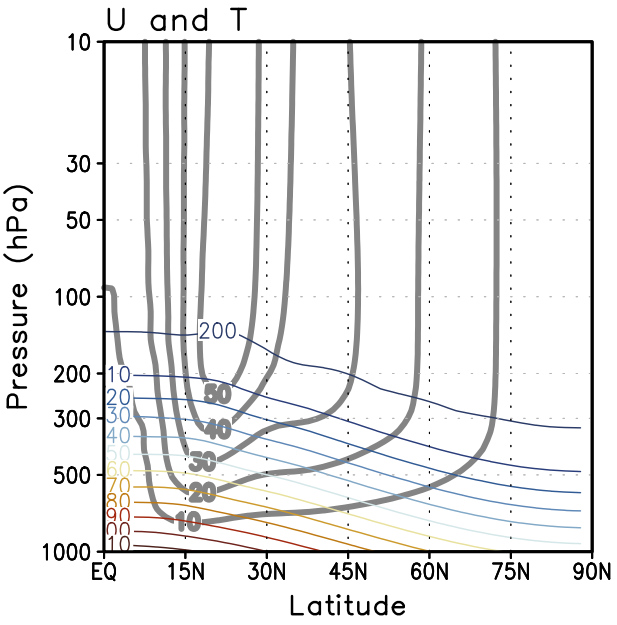

FIG. 6. Temperature (K; thin contour) and zonal wind ($\mathrm{m\,s^{-1}}$; thick gray contour) of the initial condition used for the transient simulation.

model with slightly different initial perturbations. The simple ensemble mean is used for the analysis.

Figures 7a and 7b show the time evolution of temperature and zonal wind at 114 hPa from the ensemble mean. Temperature and zonal wind change substantially during the first tens of days as baroclinic eddies grow (Fig. 7c). The temperature in the deep tropics slightly increases until 40 days, then drops quickly by 100 days and is roughly stabilized by 300 days at around 190 K. This result suggests that the formation of the CPT takes an order of 100-day time scale, which is a much longer time scale than that of synoptic-scale eddy evolution. The subtropical jets also weaken and move poleward as the CPT forms in the tropics (Fig. 7a). Note that the warming observed during the early period is due to a transient circulation response to wave forcing in the subtropical upper troposphere (e.g., Abalos et al. 2014). A transient downwelling forms in the deep tropical lower stratosphere during the initial adjustment stage (refer to Fig. 8a), and this makes the transient warming near the tropical tropopause.

Figure 8 presents the details of the CPT evolution and associated zonal-mean-flow and wave activity changes. For simplicity, the evolution process is classified into three stages. This classification is made subjectively based on the wave activity and zonal wind changes, but overall result is not sensitive to the details of the classification.

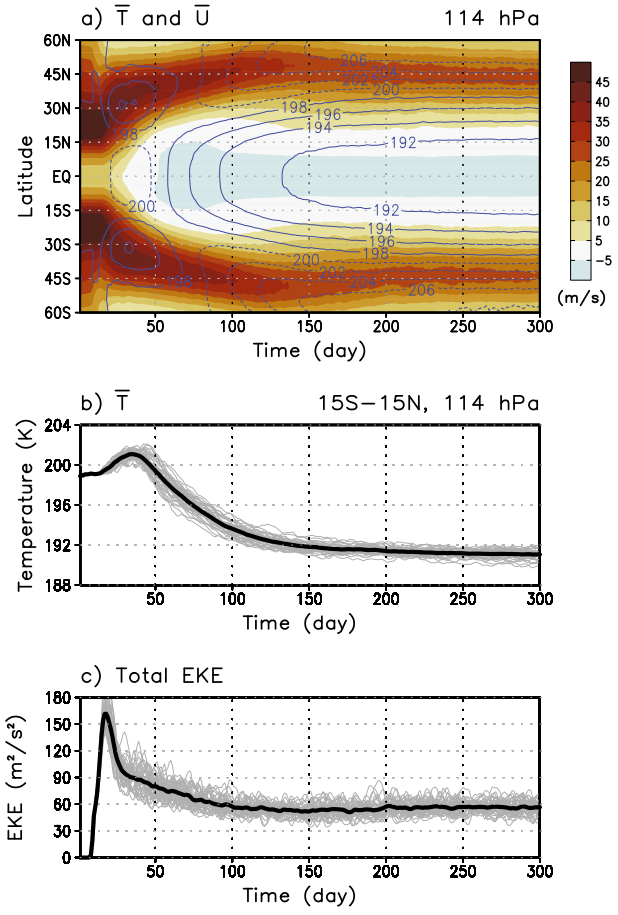

FIG. 7. Time evolution of (a) zonal-mean temperature (contour) and zonal wind (shading) at 114 hPa obtained from the ensemble mean of transient simulations. (b) Tropical-mean (15°S–15°N) temperatures at 114 hPa and (c) global-mean eddy kinetic energy. Thin lines denote individual simulations, and thick lines are their ensemble mean.

1) STAGE 1: GROWTH OF BAROCLINIC WAVES AND POLEWARD SHIFT OF THE TROPOSPHERE JET (~DAY 25)

Baroclinic waves grow rapidly in the midlatitude during the first few tens of days. They effectively transport heat from the tropics to the extratropics and deposit westerly momentum in the source region, causing the poleward shift of the tropospheric jet (Fig. 8a). Although the EP-flux divergence (shading in Fig. 8b) is negative in the midlatitude troposphere, this wave forcing is mostly compensated by the Coriolis torque of the strong poleward motion (refer to the streamlines in Fig. 8a). Note that the horizontal EP flux diverges (eddy momentum flux converges) in the midlatitude troposphere, which indicates deposits of westerly momentum in this region. The resulting jet change is largely confined within the troposphere during this stage (Figs. 8a and 8b).

2) STAGE 2: PROPAGATION OF BAROCLINIC WAVES INTO THE STRATOSPHERE AND POLEWARD SHIFT OF THE STRATOSPHERE JET (~DAY 100)

A strong westerly jet is maintained in the stratosphere for a while (refer to Figs. 8a and 8c). This westerly jet allows baroclinic waves to propagate into the stratosphere matching the Charney–Drazin criterion (Charney and Drazin 1961). The vertically propagating waves generally refract toward the equator and deposit easterly momentum on the equatorial side of the stratospheric jet, where the critical latitude is located (shading in Fig. 8d). This wave forcing and associated zonal-wind deceleration primarily appear in the lower stratosphere by 50 days (not shown), then extend gradually toward the upper stratosphere. The overturning circulation in the stratosphere (Fig. 8c) keeps accelerating the poleward side of the stratospheric jet. As a result, the poleward shift of the jet progresses in the stratosphere (~day 100). During this period, the overturning circulation extends deep into the stratosphere, and the distinct CPT starts to locate in the deep tropics (shading in Fig. 8c).

3) STAGE 3: VERTICAL CONFINEMENT OF THE WESTERLY JET

As tropospheric waves propagate farther into the upper stratosphere, the westerly jet in the upper stratosphere begins to decelerate from the top (Fig. 8e), where the critical level exists and maximum wave dissipation occurs (shading in Fig. 8f; the critical line is found near 5–10 $m\,s^{-1}$ contour lines). The resulting zonal-wind deceleration again lowers the critical level and associated wave breaking region. This successive downward movement of the zonal-wind deceleration shortens the height of the westerly jet, which results in the vertically confined westerly jet in the stratosphere (Fig. 8e). A slow but further confinement of the jet occurs by day 300. During this stage, the stratospheric circulation is concentrated in the lower stratosphere, and the associated adiabatic cooling further intensifies the localized cold region in the tropical lower stratosphere (Fig. 8e).

The temporal evolution indicates that the CPT occurs in the natural balancing process between wave forcing and zonal-mean flow in the stratosphere. The wave forcing decelerates zonal wind in the subtropical and the midlatitude lower stratosphere, and the large-scale overturning circulation forms in the stratosphere to balance this wave forcing. This overturning circulation is characterized by localized upwelling in the tropical UTLS and broad downwelling in the extratropical

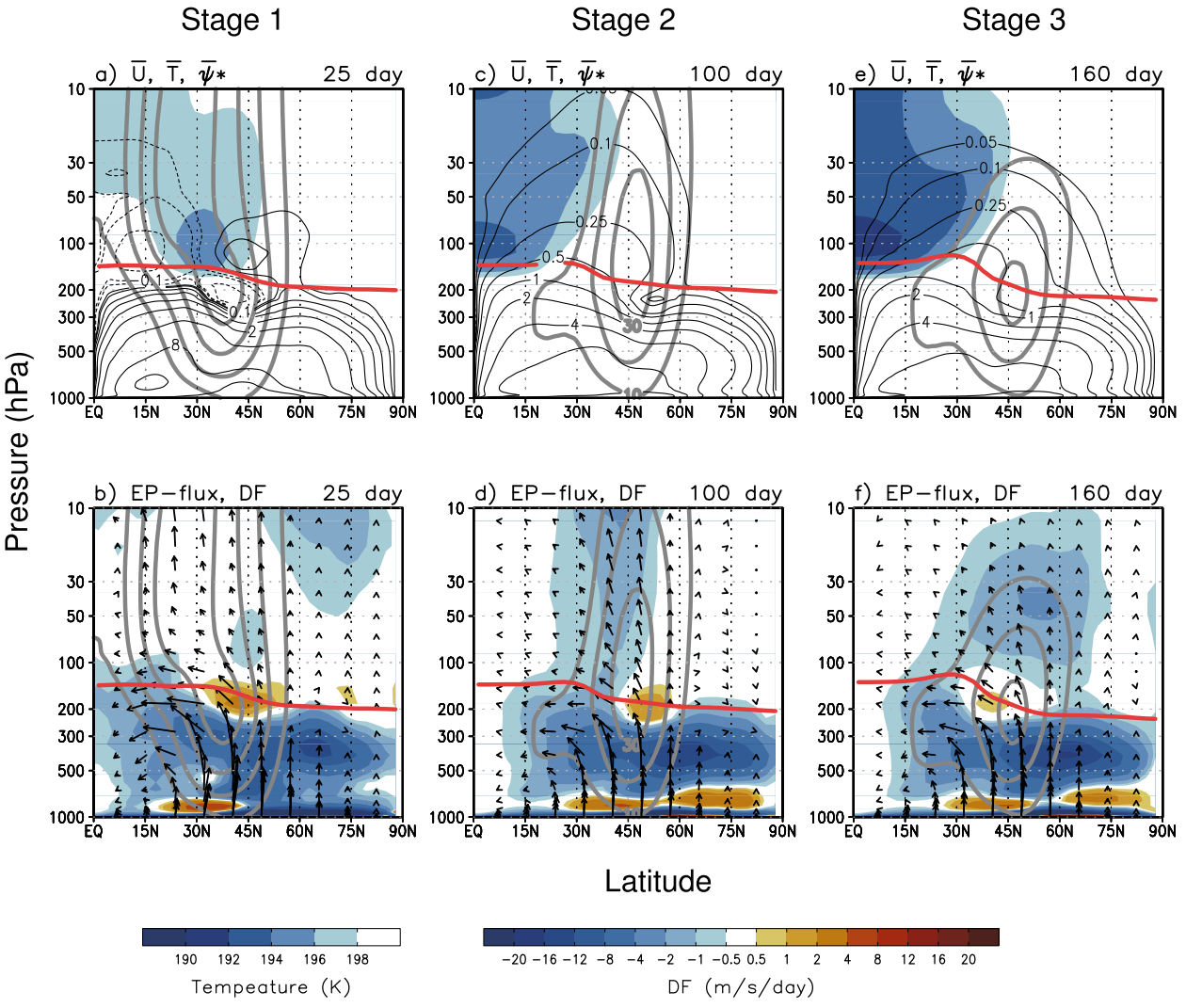

FIG. 8. Snap shots of the transient simulation at 25, 100, and 160 days obtained from the ensemble mean. (a),(c),(e) Mass streamfunction of the residual circulation (10^{10} kg s^{-1}; thin contour), zonal-mean temperature below 198 K (shading), and zonal wind (thick contour). (b),(d),(f) EP flux (vector), scaled EP-flux divergence (m s^{-1} day^{-1}; shading). Lapse-rate tropopause is presented as red curves. EP-flux vectors are scaled in height by multiplying by $e^{z/H}$ for visual clarity.

stratosphere, and the tropical part of the circulation causes the formation of the CPT in the model. This feature resembles the shallow branch of the BDC observed in the real atmosphere.

One interesting aspect of this process is development of the reversed meridional temperature gradient in the UTLS. Because of the formation of the CPT in the tropics, the meridional temperature gradient in the midlatitude changes its sign at around 200 hPa (see Fig. 1b). This reversed temperature gradient should be balanced by vertically decreasing westerly wind in the midlatitudes (through thermal wind balance) and makes the vertically confined westerly jet in the lower stratosphere. This vertical structure of the westerly limits the vertical propagation of Rossby wave and thus induces shallow wave forcing in the lower stratosphere. In this way, the CPT maintains its shallow vertical structure.

4. Sensitivity tests

The overall findings may be sensitive to the choice of model resolution and the T_e profile. Likewise, the results may also change in the presence of planetary-scale wave sources. In this section, the robustness of the results is further tested by changing the model resolution, the T_e profile, and surface boundary conditions.

a. Model resolution

The sensitivity to the model resolution is tested with varying horizontal and vertical resolutions. Specifically, the model is integrated with the HS T_e at T21, T42, T85, and T127 resolutions with 40 vertical levels (L40, hereinafter) or at T42 resolution with L20, L40, L80, and L160 levels. The vertical resolution is roughly equally increased in all levels. The results are summarized in Figs. 9a,b in terms of the tropical-mean (15°S–15°N) temperature profiles. All simulations exhibit the distinct CPT with quantitatively similar temperatures unless the model resolution is lowered to T21 or L20. This indicates that the overall results are quite robust to the resolution. In comparison to the control T42L40 run, T85 or L80 runs show slightly colder CPT temperatures, but the results present good convergence with higher resolution. Both L80 and L160 runs show small temperature departure from the T_e in the middle stratosphere, which results in a more vertically confined CPT compared to that of L40. This result may suggest that a higher vertical resolution is needed to better represent the vertical profile of wave-driven upwelling in the mid- to upper stratosphere.

b. T_e profile

To examine the sensitivity to the T_e profile, the T_e profile used in SW is tested as described in section 2c. With the SW T_e profile, two experiments are performed with different Δ_h and surface temperature at the equator T_0. All other parameters are identical to those used in the Earth-like simulation in SW. Note that $T_0 = 360\,\mathrm{K}$, $\Delta_h = 90\,\mathrm{K}$ run is equivalent to $\tilde{T}_s^e = 260\,\mathrm{K}$, $\Delta_h = 90\,\mathrm{K}$ in SW.

The SW runs also reproduce the well-defined CPT (Fig. 9c). Interestingly, the resulting CPT temperature is colder than that of the control run (the HS T_e with $\Delta_h = 60\,\mathrm{K}$ and $\Delta_v = 10\,\mathrm{K}$). This CPT temperature is not directly caused by the convective adjustment because the convective adjustment in the model cools the lower troposphere but heats the upper troposphere when temperature profile is unstable (SW). It is instead caused by wave-driven upwelling as in the control run. Although a direct comparison between the HS and SW simulations is difficult because they use different processes in setting the T_e, the westerly jet in the SW run is located at lower latitudes and more confined in the lower stratosphere compared to that in the control run (not shown).

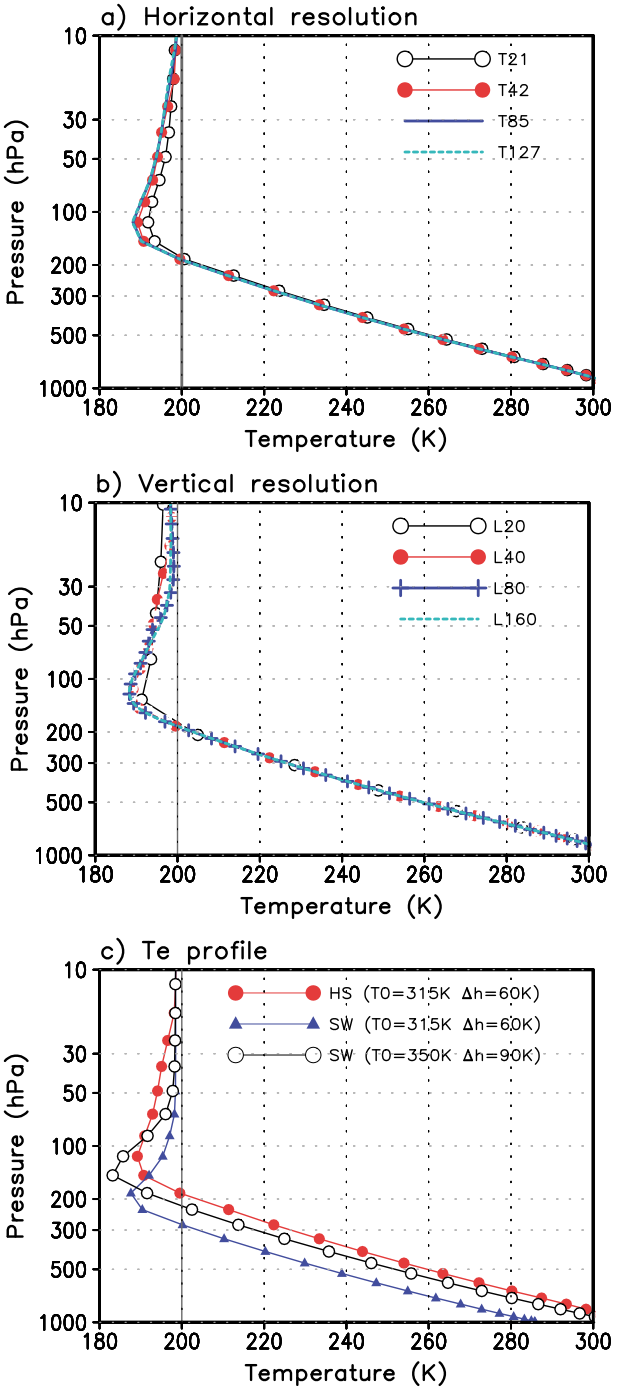

FIG. 9. Temperature profiles averaged over the deep tropics (15°S–15°N) for different (a) horizontal resolutions (T21, T42, T85, and T127), (b) vertical resolutions (L20, L40, L80, and L160), and (c) equilibrium temperature profiles (HS and SW).

c. Planetary-scale wave source

All simulations discussed so far are performed with flat surface boundary condition. To test the potential impact of stationary waves on the formation of the CPT, the model is integrated with large-scale topography. Specifically, simulations are made with a sinusoidal topography of zonal wavenumber 1 or 2 as described in

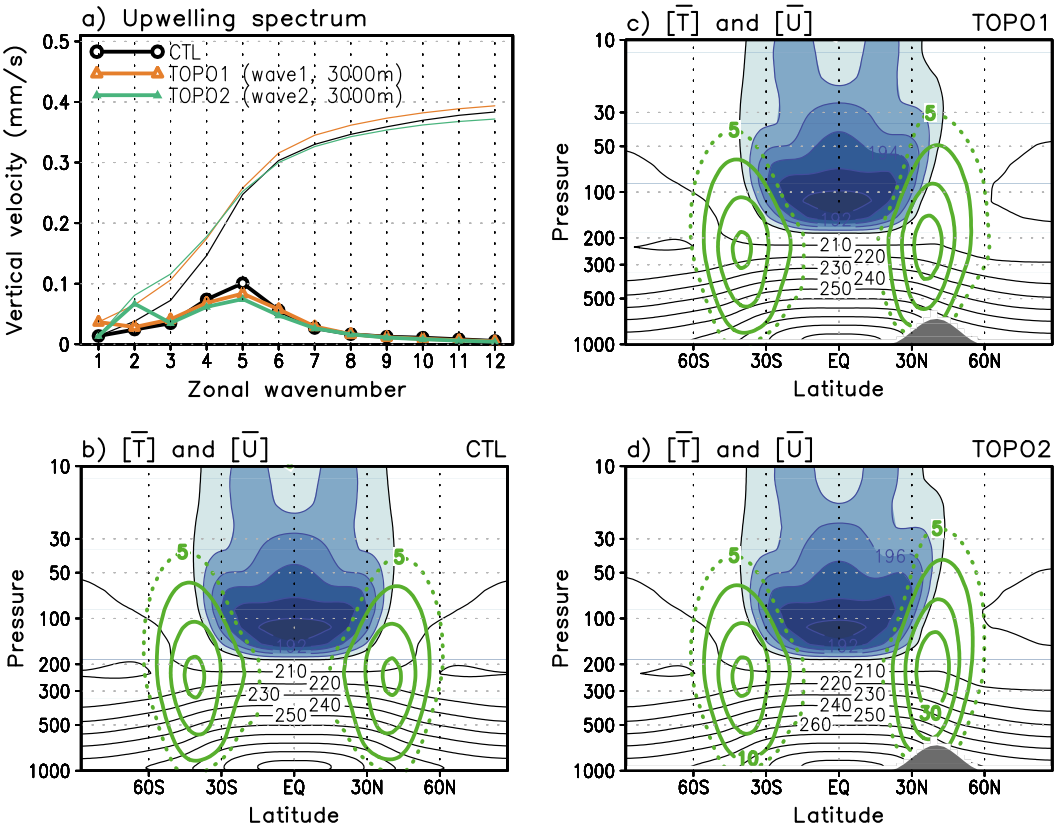

FIG. 10. (a) Spectrum of tropical-mean (15°S–15°N) upwelling at 114 hPa (thick lines) as a function of zonal wavenumber for control simulation (black) and simulations with wavenumber-1 (TOPO1; orange) and -2 (TOPO2; green) topographies. Zonal-mean climatology as in Fig. 1b from (b) control, (c) TOPO1, and (d) TOPO2 simulations.

Gerber and Polvani (2009). To efficiently generate planetary waves, the topography is centered at 40°N (covering 20°–60°N) where the maximum surface westerly is located.

The introduction of the topography makes notable changes in the tropospheric wave spectrum; thus, a corresponding change in upwelling is expected. Figure 10a shows portion of tropical upwelling that is driven by individual wave forcings decomposed by zonal wavenumber. The results from 3-km topography are shown here. The accumulation of each wave's contribution becomes total upwelling when the wavenumber is sufficiently large (Fig. 10a thin lines). Interestingly, the result shows that the introduced topography does not significantly change total wave-driven upwelling at the modeled CPT, although planetary-scale wave activity is much stronger in topography experiments compared to that in control run (Fig. 10a). As such, CPT temperatures are roughly the same in the topography and the control runs (Figs. 10b–d). It should be noted that the relative contribution of planetary-scale waves versus synoptic-scale waves is notably modified by the large-scale topography. In the absence of topography, tropical upwelling is simply dominated by synoptic-scale waves of wavenumbers 4–6 as described in the previous section (e.g., Fig. 4b). This synoptic-wave contribution is significantly reduced when wavenumber-1 or -2 topography is introduced in the model. Although not shown, qualitatively similar results (i.e., no net change in total upwelling but redistribution of its wave spectrum) are obtained with varying topography height.

The above result suggests that the CPT temperature is not sensitive to forced planetary-scale waves in the model. Although the partitioning between planetary-scale and synoptic-scale waves is changed by the surface boundary condition, the total wave activities in the lower stratosphere are qualitatively same in this simulation. In fact, Yu and Hartmann (1995) and Son et al. (2009) have shown that, regardless of the topography, the total eddy kinetic energy is largely conserved in the dynamic-core GCM if the available potential energy is fixed. Physically, the small sensitivity of upwelling to planetary-scale wave sources can be understood as a simple compensation of synoptic-scale wave forcing by

planetary-scale one in the mechanism of wave-driven upwelling.

It is worth noting that the aforementioned sensitivity might change if a strong westerly (waveguide) exists in the stratosphere as in the Northern Hemisphere winter. As hinted from Figs. 10c and 10d, which shows a slightly deeper cold region into the stratosphere in the presence of the topography, planetary-scale waves tend to propagate deeper and make a vertically extended BDC than synoptic-scale waves do. They propagate even higher when strong westerly prevails in the stratosphere and drives a deep meridional circulation covering the whole stratosphere. The deep branch of the BDC may have less effect at the tropical tropopause compared to the shallow branch; thus, the roughly equal compensation shown in this experiment may not happen.

5. Summary and discussion

Several mechanisms have been proposed in the literature to explain the formation and maintenance of the CPT. They include radiative processes and radiative–convective processes and wave-driven circulations by both the tropical and extratropical waves. Among them, the role of wave-driven circulation, focusing on tropical upwelling, is examined using synoptic-scale wave forcing in a series of dry dynamic-core GCM experiments.

The well-defined CPT is found in the idealized simulation. This result indicates that the CPT can be produced by baroclinic eddies without comprehensive moist and radiative processes. In the model, the CPT is maintained by adiabatic cooling from wave-driven upwelling near the tropical tropopause. This upwelling, which is a part of the BDC in the model, is primarily caused by mechanical drag from synoptic-scale wave dissipation (shown by the EP-flux convergence) in the subtropical and midlatitude lower stratosphere. A series of sensitivity tests further confirms that tropical upwelling and temperature at the CPT are systematically related to background baroclinicity of the model.

As expected, the CPT disappears in the axisymmetric (2D and eddy-free) model simulations. The transient simulation from the axisymmetric initial condition to the eddy-permitting state (3D) showed that the formation of the CPT is a part of balancing process between wave forcing and large-scale mean-flow responses in the lower stratosphere. Wave forcing in the lower stratosphere induces the tropical cold point through the stratospheric overturning circulation. In turn, the cold point limits further the region of wave breaking to the lower stratosphere by modifying vertical structure of the westerly jet. The shallow vertical structure of the CPT and overturning circulation in the lower stratosphere can partly be understood with this process. It is also found that planetary-scale waves forced by topography do not significantly change simulated tropical upwelling and temperature at the CPT, in contrast to the effect of background baroclinicity change. The topography forcing only modifies the wave spectrum of upwelling in the simulation.

The presence of the CPT could be one of the fundamental reasons why the midlatitude jet is confined within the troposphere and lower stratosphere. Without the CPT, the meridional temperature gradient in the midlatitudes does not change its sign rapidly in height; thus, the associated zonal wind should extend into the deep stratosphere via the thermal wind balance. In this sense, the formation of the CPT and related dynamic and thermodynamic processes are also important for understanding the structure of the westerly jet in the midlatitudes.

Since the HS forcing assumes the equinoctial condition with no temperature gradient in the stratosphere, the model results may be compared to observations during the equinoctial months. Figure 11 shows the climatological zonal-mean zonal wind and EP flux during March–May derived from ERA-Interim. In this season, the tropospheric jets in both hemispheres extend high into the lower stratosphere (Fig. 11a), which is qualitatively similar to the modeled jet in Fig. 1b. The EP flux and its divergence (Fig. 11c) in the upper troposphere and stratosphere are also qualitatively similar to those in the model (Fig. 3b). The decomposition of wave forcing into planetary-scale (Fig. 11b) and synoptic- and smaller-scale components (Fig. 11d) reveals that contribution by nonplanetary waves is significantly large in the UTLS. Particularly, in the subtropical lower stratosphere (~30° in 50–100 hPa), forcing by synoptic and smaller-scale waves is comparable or even larger than that of planetary-scale waves (see the bottom panel of Figs. 11b,d).

Figure 12 presents the contribution of planetary and nonplanetary waves to upwelling in the deep tropic (15°S–15°N) computed from the reanalysis data. In the deep tropics, planetary-scale waves have a larger contribution to upwelling than synoptic and smaller-scale (mostly synoptic scale) waves do in all seasons. However, it is also evident that the synoptic and smaller-scale waves are also important for maintaining tropical upwelling. It is worth noting that the model experiments with 3-km topography still underestimate planetary-scale wave driving (Fig. 12). It seems due to lack of other planetary-scale wave sources, such as tropical deep convection and land–sea contrast.

It is clear that wave-driven upwelling significantly contributes to the formation and maintenance of the CPT. However, the scale, origins, and types of waves involved in

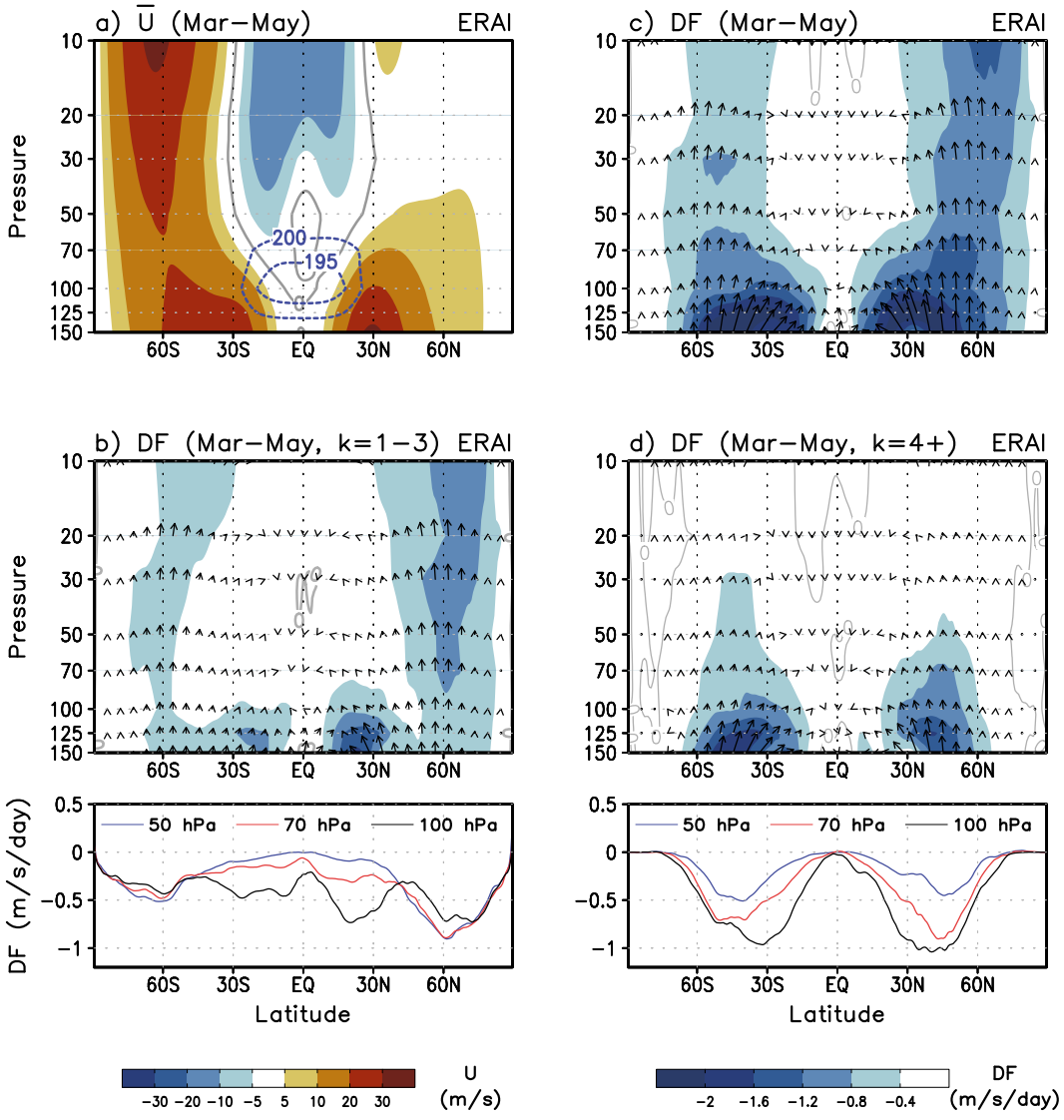

FIG. 11. (a) Zonal-mean zonal wind ($m\,s^{-1}$) and (c) EP flux and scaled EP-flux divergence ($m\,s^{-1}\,day^{-1}$) climatology (1979–2012) for March–May computed from ERA-Interim. The CPT region is denoted by zonal-mean temperature (dashed contour; 195, 200 K). EP flux and scaled EP-flux divergence of (b) planetary-scale waves (wavenumbers 1–3) and (d) synoptic-scale waves (wavenumbers 4+). (bottom) The scaled EP-flux divergence at 50, 70, and 100 hPa by (left) planetary- and (right) synoptic-scale waves. EP-flux vectors are scaled in height by multiplying by $e^{z/H}$ for visual clarity.

this process are still important issues that remain to be understood (Fueglistaler et al. 2009; Randel and Jensen 2013). In addition, interactions between different types of waves through mean-flow change is also poorly known (e.g., the mean-flow change by planetary-scale waves can alter the propagation of synoptic-scale waves). These issues may be addressed through comprehensive model experiments with realistic wave sources and background conditions in the troposphere and stratosphere.

It is important to recall that the present study does not consider convective and realistic radiative processes. Particularly, tropical convection and the associated equatorial waves are important in setting the horizontal structure of the CPT (Gettelman and Birner 2007; Fueglistaler et al. 2009). They also play important roles in sharpening the CPT (e.g., Kim and Son 2012; Paulik and Birner 2012) and enhancing tropical upwelling in the UTLS (e.g., Kerr-Munslow and Norton 2006; Ortland and Alexander 2014; Virts and Wallace 2014). The height of the CPT and its sharpness are also partly influenced by the radiative processes (e.g., Thuburn and Craig 2000). These missing convective and radiative

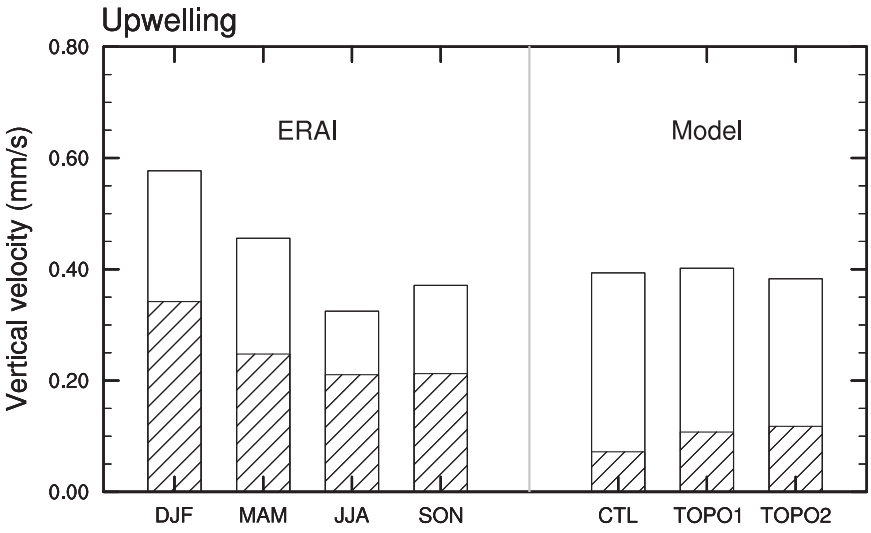

FIG. 12. Tropical-mean (15°S–15°N) $\langle \overline{w}^*_{\mathrm{DF}} \rangle$ climatology (1979–2012) at 100 hPa estimated from ERA-Interim for each season, and $\langle \overline{w}^*_{\mathrm{DF}} \rangle$ at 114 hPa from control (CTL), wavenumber-1 (TOPO1) and -2 topography (TOPO2) experiments. Contribution of planetary-scale waves (wavenumbers 1–3) is denoted by hatching.

processes may explain why the modeled temperature profile has a relatively broader peak at the CPT compared to the observation.

Acknowledgments. We thank William Randel, Thomas Birner, Louis Rivoire, and two anonymous reviewers for their helpful comments on this manuscript. Their suggestions significantly improved this manuscript. We also thank Jacques Derome and Hai Lin for constructive discussion during the initial phase of this project. This work was supported by Korean Ministry of Environment through "Climate Change Correspondence Program" and the Basic Science Research Program through the National Research Foundation of Korea (NRF) funded by the Ministry of Education (2013R1A1A1006530).

REFERENCES

Abalos, M., W. J. Randel, D. E. Kinnison, and E. Serrano, 2013: Quantifying tracer transport in the tropical lower stratosphere using WACCM. *Atmos. Chem. Phys.,* **13,** 10 591–10 607, doi:10.5194/acp-13-10591-2013.

——, ——, and E. Serrano, 2014: Dynamical forcing of subseasonal variability in the tropical Brewer–Dobson circulation. *J. Atmos. Sci.,* **71,** 3439–3453, doi:10.1175/JAS-D-13-0366.1.

Andrews, D. G., J. R. Holton, and C. B. Leovy, 1987: *Middle Atmosphere Dynamics.* International Geophysics Series, Vol. 40, Academic Press, 489 pp.

Birner, T., 2010: Residual circulation and tropopause structure. *J. Atmos. Sci.,* **67,** 2582–2600, doi:10.1175/2010JAS3287.1.

——, and H. Bönisch, 2011: Residual circulation trajectories and transit times into the extratropical lowermost stratosphere. *Atmos. Chem. Phys.,* **11,** 817–827, doi:10.5194/acp-11-817-2011.

Bordoni, S., and T. Schneider, 2010: Regime transitions of steady and time-dependent Hadley circulations: Comparison of axisymmetric and eddy-permitting simulations. *J. Atmos. Sci.,* **67,** 1643–1654, doi:10.1175/2009JAS3294.1.

Branscome, L., W. J. Gutowski Jr., and D. Stewart, 1989: Effect of surface fluxes on the nonlinear development of baroclinic waves. *J. Atmos. Sci.,* **46,** 460–475, doi:10.1175/1520-0469(1989)046<0460:EOSFOT>2.0.CO;2.

Brewer, A., 1949: Evidence for a world circulation provided by the measurements of helium and water vapour distribution in the stratosphere. *Quart. J. Roy. Meteor. Soc.,* **75,** 351–363, doi:10.1002/qj.49707532603.

Butler, A. H., D. W. J. Thompson, and R. Heikes, 2010: The steady-state atmospheric circulation response to climate change–like thermal forcings in a simple general circulation model. *J. Climate,* **23,** 3474–3496, doi:10.1175/2010JCLI3228.1.

Charney, J. G., and P. G. Drazin, 1961: Propagation of planetary-scale disturbances from the lower into the upper atmosphere. *J. Geophys. Res.,* **66,** 83–109, doi:10.1029/JZ066i001p00083.

Chen, G., and P. Zurita-Gotor, 2008: The tropospheric jet response to prescribed zonal forcing in an idealized atmospheric model. *J. Atmos. Sci.,* **65,** 2254–2271, doi:10.1175/2007JAS2589.1.

——, and L. Sun, 2011: Mechanisms of the tropical upwelling branch of the Brewer–Dobson circulation: The role of extratropical waves. *J. Atmos. Sci.,* **68,** 2878–2892, doi:10.1175/JAS-D-11-044.1.

Davis, S. M., C. K. Liang, and K. H. Rosenlof, 2013: Interannual variability of tropical tropopause layer clouds. *Geophys. Res. Lett.,* **40,** 2862–2866, doi:10.1002/grl.50512.

Dickinson, R., 1968: Planetary Rossby waves propagating vertically through weak westerly wind wave guides. *J. Atmos. Sci.,* **25,** 984–1002, doi:10.1175/1520-0469(1968)025<0984:PRWPVT>2.0.CO;2.

Dobson, G. M. B., 1956: Origin and distribution of the polyatomic molecules in the atmosphere. *Proc. Roy. Soc. London,* **A236,** 187–193, doi:10.1098/rspa.1956.0127.

Forster, P. M. de F., and K. P. Shine, 2002: Assessing the climate impact of trends in stratospheric water vapor. *Geophys. Res. Lett.,* **29,** doi:10.1029/2001GL013909.

Fueglistaler, S., A. E. Dessler, T. J. Dunkerton, I. Folkins, Q. Fu, and P. W. Mote, 2009: Tropical tropopause layer. *Rev. Geophys.,* **47,** RG1004, doi:10.1029/2008RG000267.

Garcia, R., 1987: On the mean meridional circulation of the middle atmosphere. *J. Atmos. Sci.,* **44,** 3599–3609, doi:10.1175/1520-0469(1987)044<3599:OTMMCO>2.0.CO;2.

Garny, H., M. Dameris, W. Randel, G. E. Bodeker, and R. Deckert, 2011: Dynamically forced increase of tropical upwelling in the lower stratosphere. *J. Atmos. Sci.,* **68,** 1214–1233, doi:10.1175/2011JAS3701.1.

Gerber, E. P., and L. M. Polvani, 2009: Stratosphere–troposphere coupling in a relatively simple AGCM: The importance of stratospheric variability. *J. Climate,* **22,** 1920–1933, doi:10.1175/2008JCLI2548.1.

Gettelman, A., and T. Birner, 2007: Insights into tropical tropopause layer processes using global models. *J. Geophys. Res.,* **112,** D23104, doi:10.1029/2007JD008945.

——, M. L. Salby, and F. Sassi, 2002: Distribution and influence of convection in the tropical tropopause region. *J. Geophys. Res.,* **107,** doi:10.1029/2001JD001048.

——, P. M. Forster, M. Fujiwara, Q. Fu, H. Vömel, L. K. Gohar, C. Johanson, and M. Ammerman, 2004: Radiation balance of the tropical tropopause layer. *J. Geophys. Res.,* **109,** D07103, doi:10.1029/2003JD004190.

Grise, K. M., and D. W. J. Thompson, 2013: On the signatures of equatorial and extratropical wave forcing in tropical tropopause layer temperatures. *J. Atmos. Sci.,* **70,** 1084–1102, doi:10.1175/JAS-D-12-0163.1.

Haqq-Misra, J., S. Lee, and D. M. W. Frierson, 2011: Tropopause structure and the role of eddies. *J. Atmos. Sci.,* **68,** 2930–2944, doi:10.1175/JAS-D-11-087.1.

Haynes, P. H., M. E. McIntyre, T. G. Shepherd, C. J. Marks, and K. P. Shine, 1991: On the "downward control" of extratropical diabatic circulations by eddy-induced mean zonal forces. *J. Atmos. Sci.,* **48,** 651–679, doi:10.1175/1520-0469(1991)048<0651:OTCOED>2.0.CO;2.

Held, I. M., and A. Hou, 1980: Nonlinear axially symmetric circulations in a nearly inviscid atmosphere. *J. Atmos. Sci.,* **37,** 515–533, doi:10.1175/1520-0469(1980)037<0515:NASCIA>2.0.CO;2.

——, and M. J. Suarez, 1994: A proposal for the intercomparison of the dynamical cores of atmospheric general circulation models. *Bull. Amer. Meteor. Soc.,* **75,** 1825–1830, doi:10.1175/1520-0477(1994)075<1825:APFTIO>2.0.CO;2.

Highwood, E., and B. Hoskins, 1998: The tropical tropopause. *Quart. J. Roy. Meteor. Soc.,* **124,** 1579–1604, doi:10.1002/qj.49712454911.

Holloway, C. E., and J. D. Neelin, 2007: The convective cold top and quasi equilibrium. *J. Atmos. Sci.,* **64,** 1467–1487, doi:10.1175/JAS3907.1.

Holton, J. R., P. H. Haynes, M. E. McIntyre, A. R. Douglass, R. B. Rood, and L. Pfister, 1995: Stratosphere-troposphere exchange. *Rev. Geophys.,* **33,** 403–439, doi:10.1029/95RG02097.

Johnson, R. H., and D. C. Kriete, 1982: Thermodynamic and circulation characteristics of winter monsoon tropical mesoscale convection. *Mon. Wea. Rev.,* **110,** 1898–1911, doi:10.1175/1520-0493(1982)110<1898:TACCOW>2.0.CO;2.

Kerr-Munslow, A. M., and W. A. Norton, 2006: Tropical wave driving of the annual cycle in tropical tropopause temperatures. Part I: ECMWF analyses. *J. Atmos. Sci.,* **63,** 1410–1419, doi:10.1175/JAS3697.1.

Kim, H.-K., and S. Lee, 2001: Hadley cell dynamics in a primitive equation model. Part I: Axisymmetric flow. *J. Atmos. Sci.,* **58,** 2845–2858, doi:10.1175/1520-0469(2001)058<2845:HCDIAP>2.0.CO;2.

Kim, J., and S.-W. Son, 2012: Tropical cold-point tropopause: Climatology, seasonal cycle, and intraseasonal variability derived from COSMIC GPS radio occultation measurements. *J. Climate,* **25,** 5343–5360, doi:10.1175/JCLI-D-11-00554.1.

Kuang, Z., and C. S. Bretherton, 2004: Convective influence on the heat balance of the tropical tropopause layer: A cloud-resolving model study. *J. Atmos. Sci.,* **61,** 2919–2927, doi:10.1175/JAS-3306.1.

Küpper, C., J. Thuburn, G. C. Craig, and T. Birner, 2004: Mass and water transport into the tropical stratosphere: A cloud-resolving simulation. *J. Geophys. Res.,* **109,** D10111, doi:10.1029/2004JD004541.

Labitzke, K. G., and H. van Loon, 1999: *The Stratosphere: Phenomena, History, and Relevance.* Springer, 179 pp.

Manabe, S., and R. F. Strickler, 1964: Thermal equilibrium of the atmosphere with a convective adjustment. *J. Atmos. Sci.,* **21,** 361–385, doi:10.1175/1520-0469(1964)021<0361:TEOTAW>2.0.CO;2.

Mote, P. W., and Coauthors, 1996: An atmospheric tape recorder: The imprint of tropical tropopause temperatures on stratospheric water vapor. *J. Geophys. Res.,* **101,** 3989–4006, doi:10.1029/95JD03422.

Ortland, D. A., and M. J. Alexander, 2014: The residual-mean circulation in the tropical tropopause layer driven by tropical waves. *J. Atmos. Sci.,* **71,** 1305–1322, doi:10.1175/JAS-D-13-0100.1.

Paulik, L. C., and T. Birner, 2012: Quantifying the deep convective temperature signal within the tropical tropopause layer (TTL). *Atmos. Chem. Phys.,* **12,** 12 183–12 195, doi:10.5194/acp-12-12183-2012.

Plumb, R. A., 2002: Stratospheric transport. *J. Meteor. Soc. Japan,* **80,** 893–809.

——, and J. Eluszkiewicz, 1999: The Brewer–Dobson circulation: Dynamics of the tropical upwelling. *J. Atmos. Sci.,* **56,** 868–890, doi:10.1175/1520-0469(1999)056<0868:TBDCDO>2.0.CO;2.

Polvani, L. M., and P. J. Kushner, 2002: Tropospheric response to stratospheric perturbations in a relatively simple general circulation model. *Geophys. Res. Lett.,* **29,** doi:10.1029/2001GL014284.

Randel, W. J., and I. M. Held, 1991: Phase speed spectra of transient eddy fluxes and critical layer absorption. *J. Atmos. Sci.,* **48,** 688–697, doi:10.1175/1520-0469(1991)048<0688:PSSOTE>2.0.CO;2.

——, and E. J. Jensen, 2013: Physical processes in the tropical tropopause layer and their roles in a changing climate. *Nat. Geosci.,* **6,** 169–176, doi:10.1038/ngeo1733.

——, R. R. Garcia, and F. Wu, 2002: Time-dependent upwelling in the tropical lower stratosphere estimated from the zonal-mean momentum budget. *J. Atmos. Sci.,* **59,** 2141–2152, doi:10.1175/1520-0469(2002)059<2141:TDUITT>2.0.CO;2.

——, R. Garcia, and F. Wu, 2008: Dynamical balances and tropical stratospheric upwelling. *J. Atmos. Sci.,* **65,** 3584–3595, doi:10.1175/2008JAS2756.1.

Schneider, T., and C. C. Walker, 2006: Self-organization of atmospheric macroturbulence into critical states of weak nonlinear eddy–eddy interactions. *J. Atmos. Sci.,* **63,** 1569–1586, doi:10.1175/JAS3699.1.

Seidel, D. J., R. J. Ross, J. K. Angell, and G. C. Reid, 2001: Climatological characteristics of the tropical tropopause as

revealed by radiosondes. *J. Geophys. Res.,* **106,** 7857–7878, doi:10.1029/2000JD900837.

Sherwood, S. C., and A. E. Dessler, 2003: Convective mixing near the tropical tropopause: Insights from seasonal variations. *J. Atmos. Sci.,* **60,** 2674–2685, doi:10.1175/1520-0469(2003)060<2674:CMNTTT>2.0.CO;2.

Solomon, S., K. H. Rosenlof, R. W. Portmann, J. S. Daniel, S. M. Davis, T. J. Sanford, and G.-K. Plattner, 2010: Contributions of stratospheric water vapor to decadal changes in the rate of global warming. *Science,* **327,** 1219–1223, doi:10.1126/science.1182488.

Son, S.-W., and S. Lee, 2005: The response of westerly jets to thermal driving in a primitive equation model. *J. Atmos. Sci.,* **62,** 3741–3757, doi:10.1175/JAS3571.1.

——, and L. M. Polvani, 2007: Dynamical formation of an extratropical tropopause inversion layer in a relatively simple general circulation model. *Geophys. Res. Lett.,* **34,** L17806, doi:10.1029/2007GL030564.

——, S. Lee, and S. B. Feldstein, 2007: Intraseasonal variability of the zonal-mean extratropical tropopause height. *J. Atmos. Sci.,* **64,** 608–620, doi:10.1175/JAS3855.1.

——, M. Ting, and L. M. Polvani, 2009: The effect of topography on storm-track intensity in a relatively simple general circulation model. *J. Atmos. Sci.,* **66,** 393–411, doi:10.1175/2008JAS2742.1.

Thuburn, J., and G. C. Craig, 2000: Stratospheric influence on tropopause height: The radiative constraint. *J. Atmos. Sci.,* **57,** 17–28, doi:10.1175/1520-0469(2000)057<0017:SIOTHT>2.0.CO;2.

——, and ——, 2002: On the temperature structure of the tropical substratosphere. *J. Geophys. Res.,* **107,** doi:10.1029/2001JD000448.

Ueyama, R., E. P. Gerber, J. M. Wallace, and D. M. W. Frierson, 2013: The role of high-latitude waves in the intraseasonal to seasonal variability of tropical upwelling in the Brewer–Dobson circulation. *J. Atmos. Sci.,* **70,** 1631–1648, doi:10.1175/JAS-D-12-0174.1.

Virts, K. S., and J. M. Wallace, 2014: Observations of temperature, wind, cirrus, and trace gases in the tropical tropopause transition layer during the MJO. *J. Atmos. Sci.,* **71,** 1143–1157, doi:10.1175/JAS-D-13-0178.1.

Yu, J.-Y., and D. L. Hartmann, 1995: Orographic influences on the distribution and generation of atmospheric variability in a GCM. *J. Atmos. Sci.,* **52,** 2428–2443, doi:10.1175/1520-0469(1995)052<2428:OIOTDA>2.0.CO;2.

Yulaeva, E., J. Holton, and J. Wallace, 1994: On the cause of the annual cycle in tropical lower-stratospheric temperatures. *J. Atmos. Sci.,* **51,** 169–169, doi:10.1175/1520-0469(1994)051<0169:OTCOTA>2.0.CO;2.